PERGAMON

International Journal of Heat and Mass Transfer 46 (2003) 297–310

International Journal of HEAT and MASS TRANSFER

www.elsevier.com/locate/ijhmt

Convection in a horizontal rectangular duct under constant and variable property formulations

Qinghua Wang, Hoseon Yoo, Yogesh Jaluria *

Department of Mechanical and Aerospace Engineering, Rutgers, The State University of New Jersey, Piscataway, New Brunswick, NJ 08854-8058, USA

Received 11 April 2002; received in revised form 30 June 2002

Abstract

The convective laminar flow through a horizontal rectangular duct, with significant buoyancy effects, has been investigated analytically and numerically, employing the constant property (CP) model and the variable property (VP) model. The duct has a finite heated region on the bottom and three-dimensional transport is studied. The CP model employs the Boussinesq approximations and uses properties evaluated at four different reference temperatures, i.e. the ambient temperature T_0, the average temperature T_f, the integrated average temperature T_{int}, and the heat source temperature T_h. In the VP model, the density and the transport properties are computed using the state equation of an ideal gas and power law correlations, respectively. Numerical results for temperature ratio ϵ, where $\epsilon = (T_h - T_0)/T_0$, ranging from 0.033 to 2.33 are presented. The spanwise variation of the transport quantities is investigated in detail for the different models, and several interesting and important tends are obtained. These results will be of considerable value in model development for a wide variety of thermal systems and processes, where large changes in material properties are encountered.

1. Introduction

The convective flow and heat transfer in a horizontal duct has been extensively investigated numerically and experimentally. In most cases of practical interest, such as those in materials processing and electronic systems, buoyancy effects are important, the fluid properties vary with the temperature, and the continuity, momentum, and energy equations are coupled. This makes the analysis and the numerical solution very involved and time consuming. One common method used to simplify the simulation of the flow and heat transfer is the application of the Boussinesq approximations, for which all the fluid properties are assumed to be constant, except for the density variation to obtain the buoyancy force, and a linear temperature dependence of density is assumed. However, these approximations are valid only when the variation in the fluid properties due to changes in the temperature are relatively small [1].

In the literature involving three-dimensional mixed convection flow, far more papers have adopted the Boussinesq approximations than the variable property (VP) model. Lin and co-workers [2–5] have done a lot work on this mixed convection flow experimentally and numerically. In their numerical study, the working fluid (air) was assumed to be a Boussinesq fluid, even when the Grashof number Gr was of the order 10^5. Part of the difference between the experimental results and the numerical predictions might have resulted from the inapplicability of the model. In our own previous research [6], the largest Grashof number was taken to be of order 10^4 in order to assure the validity of the constant property (CP) model. Chen and Lavine [7] investigated the combined buoyancy and forced flow convection in a duct with a small aspect ratio using the CP model. Two different flow patterns, i.e. the longitudinal rolls and transverse rolls, were obtained for very low Reynolds numbers. The Rayleigh number range was varied from 2000 to 4000. Nicolas et al. [8] presented the linear

* Corresponding author. Tel.: +1-732-445-3652/3514; fax: +1-732-445-5313/3124.

E-mail address: jaluria@jove.rutgers.edu (Y. Jaluria).

0017-9310/03/$ - see front matter
PII: S0017-9310(02)00272-7

Nomenclature

Ar	aspect ratio, $\mathrm{Ar} = W/H$
c_p	specific heat at constant pressure
C_P	pressure coefficient
Gr	Grashof number, $Gr = (g\beta H^3(T_\mathrm{h} - T_0))/kv^2$
H	channel height
k	thermal conductivity
L	dimensionless channel length
L_e	dimensionless entry channel length
L_h	dimensionless length of heat source
L_0	dimensionless distance beyond the heat source
Nu	local Nusselt number
Nu_s	space-averaged Nusselt number
Nu_t	time-averaged local Nusselt number
p	pressure
P	dimensionless pressure
Pr	Prandtl number, $Pr = v/\alpha$
Re	Reynolds number, $Re = u_\mathrm{m}H/v$
t	time
T	temperature
T_0	temperature of the inflow fluid
T_f	average temperature, $T_\mathrm{f} = (T_0 + T_\mathrm{h})/2$
T_h	temperature of heat source
T_int	integrated average temperature
T_ref	reference temperature
u,v,w	dimensionless velocity components in the x, y, and z directions, respectively
u_dev	velocity in fully developed flow
u_m	average inflow velocity
W	width of the channel
x,y,z	Cartesian coordinates

Greek symbols

α	thermal diffusivity
β	volumetric thermal expansion coefficient
ϵ	temperature ratio, $\epsilon = (T_\mathrm{h} - T_0)/T_0$
ρ	density
δ_{ij}	Kronecker delta
θ	dimensionless temperature, $\theta = (T - T_0)/(T_\mathrm{h} - T_0)$
μ	viscosity
v	kinematic viscosity
τ	dimensionless time, $\tau = (tu_\mathrm{m}/H)$

Superscript

$\hat{}$	dimensional variable

stability analysis of a fully developed Poiseuille flow in a duct, and a stability diagram was obtained.

The CP model might be in considerable error in some situations, in which the range of temperature variation is large. Such situations are often encountered in applications like chemical vapor deposition (CVD) and cooling of high capacity electronic systems. Jensen [9] reviewed the flow phenomena in CVD processes, and suggested that the simulation model should include temperature dependence of the fluid properties. In Spall's research [10], the viscosity and the density of the fluid were calculated using the Sutherland's law and the ideal gas law, respectively, while the Prandtl number and specific heat were assumed to be constant. Thus, it was not a complete VP model. With this model, the flow with a relative high temperature ratio ($\epsilon = 2.33$) was simulated. Nesreddine et al. [11] simulated the mixed convection transport in vertical tubes using almost the same method as Spall's except that the density was calculated by a linear approximation of the temperature dependence. Evans and Greif [12,13] did not use the Boussinesq approximations, but all fluid properties except the density were assumed to be constant, so their model was largely applicable to a CP fluid. They investigated the flow and heat transfer in CVD reactors for both a small temperature ratio ($\epsilon = 0.01$) and a high temperature ratio ($\epsilon = 2.33$).

Although work has been done on the mixed convection flow through a horizontal duct employing CP and VP models, not much effort has been directed at comparing the numerical results from the two different approaches. Chiu et al. [14] investigated the CVD process for silicon, and found that the CP model was only valid under certain limited conditions. The results from the CP model, with different reference temperatures, were presented. However, in both models, the flow was assumed to be two-dimensional and in steady state. In the present study, all the fluid properties are assumed to be dependent on temperature in the VP model, and the two models are used to simulate three-dimensional duct flow. The limitations of the CP model with Boussinesq approximations are investigated in detail. Time-dependent behavior of the flow is also studied. The results will be valuable in the development of analytical and numerical models for a variety of practical problems, such as those in materials processing.

2. Governing equations and boundary conditions

The system under consideration is shown in Fig. 1. The discrete heat source on the bottom is isothermal, at a uniform temperature T_h, and the top surface of the duct is kept at a lower uniform temperature T_0, the

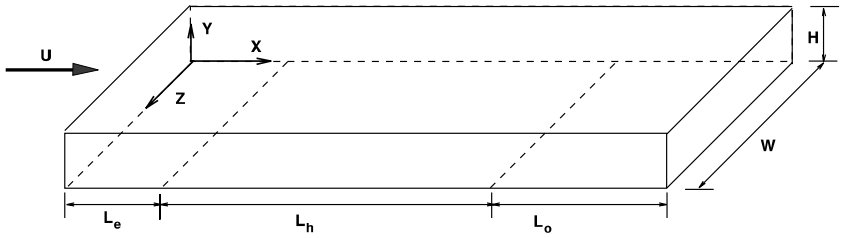

Fig. 1. A horizontal duct with a finite-sized heat source on the bottom.

temperature of the inlet flow. The side walls and other parts on the bottom are assumed to adiabatic. The entry length L_e is taken to be at a typical value of 3.0, and the length of the heated region, L_h, is fixed at 15. The tailing length L_0, beyond the heat source, is assumed to be long enough to make the Neumman conditions applicable. L_0 is chosen to be greater than 7.0 in the following calculations. The governing equations for mass, momentum, and energy conservation are as follows:

Continuity equation

$$\frac{\partial\hat{\rho}}{\partial t}+\frac{\partial(\hat{\rho}\hat{u}_j)}{\partial\hat{x}_j}=0 \tag{1}$$

Momentum equation

$$\frac{\partial(\hat{\rho}\hat{u}_i)}{\partial t}+\frac{\partial}{\partial\hat{x}_j}(\hat{\rho}\hat{u}_j\hat{u}_i)=-\frac{\partial\hat{p}}{\partial\hat{x}_i}+\frac{\partial\hat{\sigma}_{ij}}{\partial\hat{x}_j}+\hat{\rho}g_i \tag{2}$$

where

$$\hat{\sigma}_{ij}=\hat{\mu}\left(\frac{\partial\hat{u}_i}{\partial\hat{x}_j}+\frac{\partial\hat{u}_j}{\partial\hat{x}_i}\right)-\frac{2}{3}\delta_{ij}\hat{\mu}\left(\frac{\partial\hat{u}_k}{\partial\hat{x}_k}\right) \tag{3}$$

Energy equation

$$\hat{c_p}\frac{\partial(\hat{\rho}T)}{\partial t}+\hat{c_p}\frac{\partial}{\partial\hat{x}_j}(\hat{\rho}\hat{u}_jT)=\frac{\partial}{\partial\hat{x}_j}\left(\hat{k}\frac{\partial T}{\partial\hat{x}_j}\right) \tag{4}$$

The length, velocity, pressure, temperature and time are scaled, respectively, by H, $\hat{u}_{\text{avg}}$, $\hat{\rho}_0\hat{u}^2_{\text{avg}}$, T_h-T_0, and $H/\hat{u}_{\text{avg}}$. The property coefficients are nondimensionalized by the corresponding values at the ambient temperature T_0. Then dimensionless equations are obtained as follows,

$$\frac{\partial\rho}{\partial\tau}+\frac{\partial(\rho u_j)}{\partial x_j}=0 \tag{5}$$

$$\begin{aligned}\frac{\partial(\rho u_i)}{\partial\tau}+\frac{\partial}{\partial x_j}(\rho u_ju_i)=&-\frac{\partial p}{\partial x_i}+\frac{\partial}{\partial x_j}\left(\Gamma_v\frac{\partial u_i}{\partial x_j}\right)\\&+\frac{\partial}{\partial x_j}\left(\Gamma_v\frac{\partial u_j}{\partial x_i}-\frac{2}{3}\delta_{ij}\Gamma_v\frac{\partial u_k}{\partial x_k}\right)\\&+\frac{Gr}{Re^2}\frac{\rho}{\epsilon}\eta_i\end{aligned} \tag{6}$$

$$\frac{\partial(\rho\theta)}{\partial\tau}+\frac{\partial}{\partial x_j}(\rho u_j\theta)=\frac{\partial}{\partial x_j}\left(\Gamma_\theta\frac{\partial\theta}{\partial x_j}\right)+\frac{1}{PrRe}\frac{k}{c_p^2}\frac{\partial\theta}{\partial x_j}\frac{\partial c_p}{\partial x_j} \tag{7}$$

where Γ_v and Γ_θ are the diffusion coefficients in the momentum and energy equations, respectively. They have the following forms

$$\Gamma_v=\frac{\mu}{Re} \tag{8}$$

$$\Gamma_\theta=\frac{k}{c_p}\frac{1}{PrRe} \tag{9}$$

Thus the momentum and energy equations may be expressed by the general form

$$\frac{\partial(\rho\phi)}{\partial\tau}+\frac{\partial}{\partial x_j}(\rho u_j\phi)=\frac{\partial}{\partial x_j}\left(\Gamma_\phi\frac{\partial\phi}{\partial x_j}\right)+S_\phi \tag{10}$$

where Γ_ϕ and S_ϕ are summarized in Table 1.

Table 1
Summary of the variables in the governing equations

ϕ	Γ_ϕ	S_ϕ
u	Γ_v	$-\frac{\partial p}{\partial x}+\frac{\partial}{\partial x}\left(\Gamma_v\frac{\partial u}{\partial x}\right)+\frac{\partial}{\partial y}\left(\Gamma_v\frac{\partial v}{\partial x}\right)+\frac{\partial}{\partial z}\left(\Gamma_v\frac{\partial w}{\partial x}\right)-\frac{2}{3}\frac{\partial}{\partial x}(\Gamma_v\nabla\cdot\vec{v})$
v	Γ_v	$-\frac{\partial p}{\partial y}+\frac{\partial}{\partial x}\left(\Gamma_v\frac{\partial u}{\partial y}\right)+\frac{\partial}{\partial y}\left(\Gamma_v\frac{\partial v}{\partial y}\right)+\frac{\partial}{\partial z}\left(\Gamma_v\frac{\partial w}{\partial y}\right)-\frac{2}{3}\frac{\partial}{\partial y}(\Gamma_v\nabla\cdot\vec{v})-\frac{Gr}{Re^2}\frac{\rho}{\epsilon}$
w	Γ_v	$-\frac{\partial p}{\partial z}+\frac{\partial}{\partial x}\left(\Gamma_v\frac{\partial u}{\partial z}\right)+\frac{\partial}{\partial y}\left(\Gamma_v\frac{\partial v}{\partial z}\right)+\frac{\partial}{\partial z}\left(\Gamma_v\frac{\partial w}{\partial z}\right)-\frac{2}{3}\frac{\partial}{\partial z}(\Gamma_v\nabla\cdot\vec{v})$
θ	Γ_θ	$\frac{1}{PrRe}\frac{k}{c_p^2}\frac{\partial\theta}{\partial x_j}\frac{\partial c_p}{\partial x_j}$

If the Boussinesq approximations are applied, the governing equations are simplified to more convenient forms, as described in the earlier paper [6]. The flow at the inlet is assumed to be fully developed, and the velocity is calculated using the formula given by Shah and London [15] as

$$u_{\mathrm{dev}} = \left(\frac{m+1}{m}\right)\left(\frac{n+1}{n}\right)(1-|2Y-1|^n) \times \left(1-\left|\frac{2Z}{\mathrm{Ar}}-1\right|^m\right) \tag{11}$$

where m and n are constants dependent on the lateral aspect ratio, W/H, of the duct. Then the inlet boundary conditions can be expressed as

$$u = u_{\mathrm{dev}}, \quad v = w = \theta = 0, \quad x = 0 \tag{12}$$

At the outlet, the flow is also assumed to be fully developed, leading to the conditions

$$\frac{\partial u}{\partial x} = \frac{\partial v}{\partial x} = \frac{\partial w}{\partial x} = \frac{\partial \theta}{\partial x} = 0, \quad x = L \tag{13}$$

No-slip conditions are applied at all the solid surfaces. The side walls and the entry and outlet portions of the bottom surface are taken as adiabatic. The top surface and the heat source are kept at low and high temperatures, respectively. Therefore, the following conditions are obtained,

$$u = v = w = \frac{\partial \theta}{\partial z} = 0, \quad z = 0, \mathrm{Ar} \tag{14}$$

$$u = v = w = \theta = 0, \quad y = 1 \tag{15}$$

$$u = v = w = 0, \quad y = 0 \tag{16}$$

$$\frac{\partial \theta}{\partial y} = 0, \quad 0 \leqslant x \leqslant L_{\mathrm{e}},\ L_{\mathrm{e}} + L_{\mathrm{h}} \leqslant x \leqslant L \tag{17}$$

$$\theta = 1.0 \quad L_{\mathrm{e}} \leqslant x \leqslant L_{\mathrm{e}} + L_{\mathrm{h}} \tag{18}$$

The initial conditions for unsteady flow are

$$u = u_{\mathrm{dev}}, \quad v = w = \theta = 0, \quad \tau \leqslant 0 \tag{19}$$

For the VP model, the fluid (air) is treated as an ideal gas, and the state equation is used to calculate the density. Other transport properties are determined using the power law correlations given by Fotiadis et al. [16]. Thus, dimensionless property coefficients are obtained as

$$\rho = \frac{\hat{\rho}}{\hat{\rho}_0} = \frac{1}{\theta\epsilon + 1} \tag{20}$$

$$c_p = \frac{\widehat{c_p}}{\widehat{c_p}_0} = (\theta\epsilon + 1)^{0.104} \tag{21}$$

$$\mu = \frac{\hat{\mu}}{\hat{\mu}_0} = (\theta\epsilon + 1)^{0.65} \tag{22}$$

$$k = \frac{\hat{k}}{\hat{k}_0} = (\theta\epsilon + 1)^{0.79} \tag{23}$$

For the CP model, the transport properties are evaluated at a reference temperature. As employed for the two-dimensional simulation of Chiu et al. [14], four different reference temperatures are considered, i.e. the inflow temperature T_0, the heat source temperature T_{h}, the average temperature $T_{\mathrm{f}} = (T_0 + T_{\mathrm{h}})/2$, and the integrated average temperature T_{int}. As defined by Chiu et al. [14], the integrated average temperature T_{int} satisfies the equation

$$\int_{T_0}^{T_{\mathrm{int}}} \phi(T)\,\mathrm{d}T = \int_{T_{\mathrm{int}}}^{T_{\mathrm{h}}} \phi(T)\,\mathrm{d}T \tag{24}$$

Here, $\phi(T)$ represents the property function, which gives the transport property variation with temperature. For convenience of expression, CP(T_0), CP(T_{f}), CP(T_{h}), and CP(T_{int}) stand for the CP models based on the four reference temperatures. VP represents the VP model.

3. Numerical model and validation

The preceding partial differential equations are solved using the finite volume method with the SIMPLER algorithm. The numerical procedure for VP is quite similar to that for CP, described in an earlier work [6]. The main difference is that the fluid properties in VP have to be updated for every inner iteration (the pressure correction procedure in one time step). CP(T_0) yields exactly the same solution as that obtained from VP when the dimensionless coefficients of the properties are set as 1, i.e. $\rho = c_p = \mu = k = 1$, so that the formulation for the VP model yields the CP model if property variations are neglected, as expected.

The code is validated by simulating the mixed convection flow in a rectangular duct, uniformly heated from below, corresponding to the experiments carried out by Chiu and Rosenberger [17]. As shown in Fig. 2, the results from the two models are very close. Here the reference temperature for CP is the average temperature, i.e. $T_{\mathrm{ref}} = (T_{\mathrm{h}} + T_0)/2$. However, the temperature ratio ϵ is only 0.0676, so the results from the two models are expected to be similar. In the region close to the side walls, the three sets of data agree very well, but the difference between the numerical results and the experimental data increases in the central region of the channel. This trend is more pronounced in the figure on the right. To verify that the code is applicable to cases with different aspect ratios, the scheme is used to simulate the flow in a duct with a small aspect ratio, as described in the experimental and numerical work of Nyce et al. [18]. Very good agreement is found again. As shown in Fig. 3, the data are almost identical except in

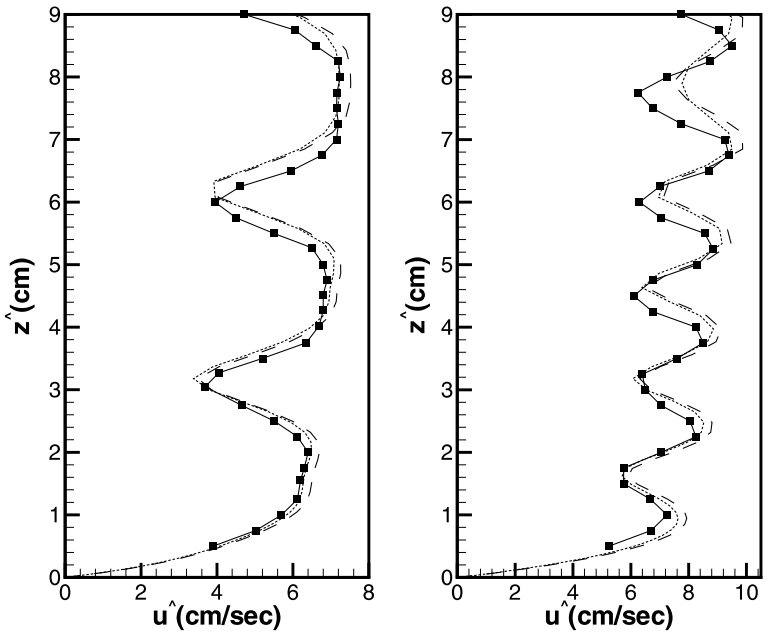

Fig. 2. Streamwise velocity $\hat{u}$ at $y = 0.2H$ (left figure) and $y = 0.5H$ (right figure) and $\hat{x} = 30$ cm in a horizontal duct. The solid line represents the experimental results in [17] and the dashed and the dotted lines represent the numerical prediction using the VP model and the CP($T_{\mathrm{ref}} = T_{\mathrm{f}}$) model, respectively.

the regions close to the crest. In the preceding two comparisons, a similarity between the two models is found. The reason is that the temperature ratio ϵ is small, and the Boussinesq approximations are satisfactory for characterizing the average behavior of the steady flow.

To determine an appropriate grid size, grid sensitivity of the solutions was evaluated for the VP model. In Table 2, the Nusselt number, space-averaged over the heat source, the maximum velocity components, the space-averaged velocity, and the pressure drop coefficient C_P are presented. In the three grid systems shown, the variables which represent average values, like $\overline{N_u}$ and C_P, change very little. For the velocity components, the peak values of the axial component u and of the transverse component w change by less than 0.5% from the medium grid size to the finest one, while by 8% from the coarsest system to the medium one. The peak value of the vertical velocity component v varies very strongly. It increases by 25.6% from the coarsest grid system to the medium one, and by 14.6% from the medium grid system to the finest system. But the global average value of the absolute value of v increases only by 9.3% and 2.2%, respectively, for the preceding grid systems. The profiles of v, given by the medium grid system, on the cross-sectional y–z plane, where the maximum values appear, agree very well with those yielded in the finest grid sytem. Moderate differences are only found in the narrow regions around the crests of v profiles. However, the computation cost for the finest system is much higher than the medium one, especially for unsteady calculations. Therefore, it is appropriate to use the medium grid system, $151 \times 21 \times 51$, in the following calculations with Ar = 5.0. In the calculation for $Re = 10$ and $\epsilon = 0.033$, excellent agreement was found between the results for $\Delta\tau = 0.01$ and for $\Delta\tau = 0.02$. Thus the time step for the unsteady calculations is fixed at $\Delta\tau = 0.02$, and larger values are used when only the steady state solution is of interest.

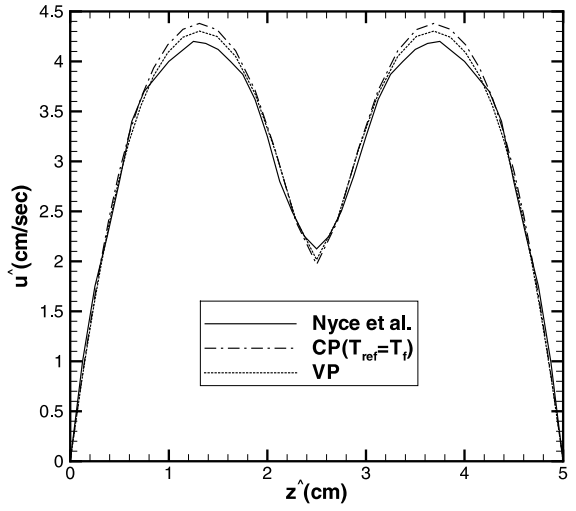

Fig. 3. Comparison of streamwise velocity $\hat{u}$ between the present prediction and that by Nyce et al. [18] at $y = 0.5H$ and $\hat{x} = 30$ cm in a duct with Ar = 2.0.

Table 2
Grid independence test for $Re = 200$, $\epsilon = 0.1667$, and $\mathrm{Ar} = 5.0$

Grid	$111 \times 11 \times 31$	$151 \times 21 \times 51$	$201 \times 31 \times 81$
$\overline{N_u}$	3.289	3.2676	3.250
$u_{\max}$	1.817	1.853	1.856
$v_{\max}$	0.359	0.451	0.517
$w_{\max}$	0.426	0.464	0.465
$\overline{u^2 + v^2 + w^2}$	1.359	1.343	1.341
C_P	3.869	4.067	4.062
$\overline{\lvert v \rvert}$	5.398×10^{-2}	5.901×10^{-2}	6.032×10^{-2}

4. Results and discussion

As mentioned earlier, a recent study employing variable properties was carried out by Spall [10]. In his research, Pr and c_p were assumed to be constant, and the thermal conductivity was calculated based on known properties. This assumption seems to make sense for air, since the specific heat c_p and the Prandtl number Pr change by only about 10% and 4%, respectively, when the working temperature varies from 300 to 1000 K. If this assumption is taken as valid, the source term in the energy equation might be eliminated. In order to make the present calculations more general, than those in [10], and to obtain more accurate solutions, this assumption is not employed in this study.

5. Small temperature ratio

First, the case with $\epsilon = 0.0333$ is investigated. Based on the definition of the temperature ratio ϵ, the temperature difference between the duct top surface and the heat source is only 10 K, since the ambient temperature T_0 is fixed at 300 K. To make it easier to present the results, the nondimensional parameters, which are used to distinguish between different cases, are evaluated at the duct inlet.

When Re is as low as 10, steady oscillations occur in the duct, as shown in Fig. 4. The space-averaged Nusselt numbers, for the different models, vary at almost the same frequency, $St \simeq 0.4$, and the time-averaged values have only a small difference. The largest difference is the one between VP and CP(T_0), which is still less than 5%.

In the present paper, the results from the VP model are taken as the accurate solution, and two variables are defined to evaluate the performance of CP models with different reference temperatures. The first is the error in the space and time-averaged Nusselt number, which is defined as

$$E_{Nu} = \frac{\oint_s |Nu - Nu_v| \, \mathrm{d}s}{\oint_s Nu_v \, \mathrm{d}s} \tag{25}$$

The second variable is used to determine the difference in the velocity field between the CP models and the VP model, and is defined as

$$E_V = \frac{\oint_\Omega \sqrt{(u-u_v)^2 + (v-v_v)^2 + (w-w_v)^2} \, \mathrm{d}\forall}{\oint_\Omega \sqrt{u_v^2 + v_v^2 + w_v^2} \, \mathrm{d}\forall} \tag{26}$$

Here, $\oint_s$ and $\oint_\Omega$ represent the integration over the entire heat source surface and space integration over the entire domain enclosed by the duct, respectively. Variables with v as the subscript represent the values from the VP model.

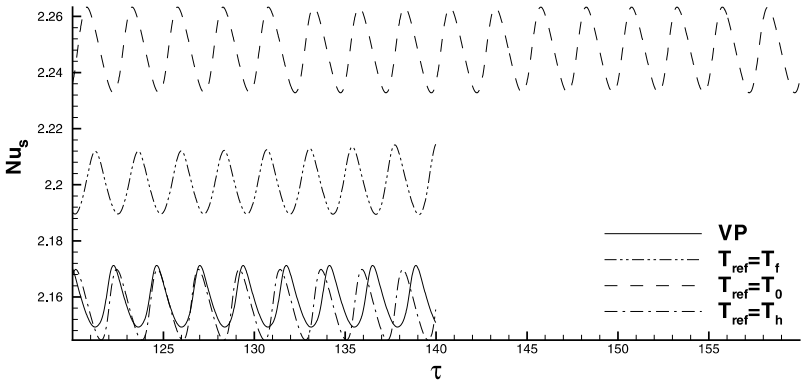

Fig. 4. Time evolution of the space-averaged Nusselt number over the heat source for $Re = 10$, and $\epsilon = 0.0333$, using different models for the analysis.

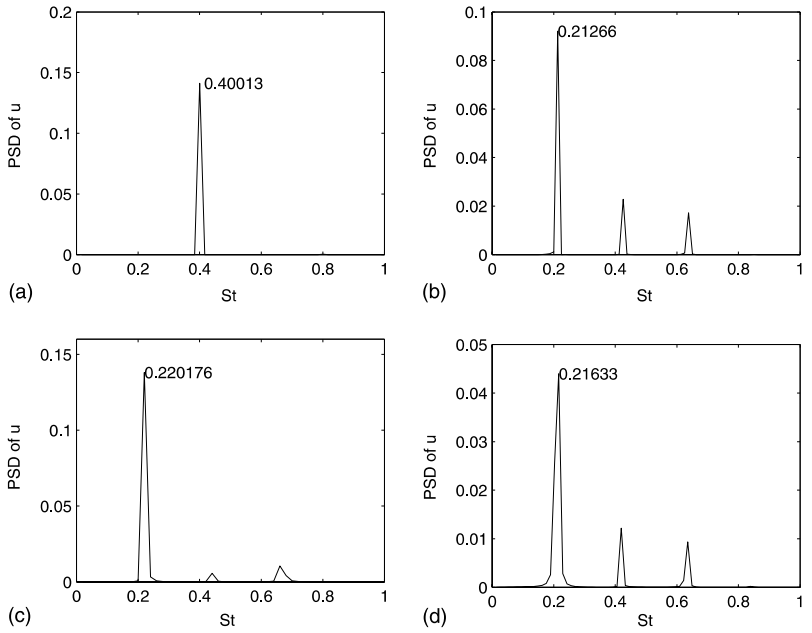

Fig. 5. PSD of the axial velocity u from the CP model with different reference temperatures for $Re = 10$ and $\epsilon = 0.033$. (a) $T_{ref} = T_0$; (b) $T_{ref} = T_f$; (c) $T_{ref} = T_h$; and (d) VP.

Based on the preceding definition, E_{Nu} for the CP models with different reference temperatures, i.e. T_0, T_f, and T_h, is 4.5%, 2.3% and 1.2%, respectively. At this point, one conclusion that may be drawn is that the CP model is accurate enough to capture the basic flow characteristics, no matter what temperature is chosen as the reference temperature. However, quantitative differences are quite significant. In order to investigate how the choice of the reference temperature affects the flow pattern, the time history of axial velocity at a point with coordinates $(18.0, 0.113, 1.456)$ is recorded. Using the fast Fourier transform (FFT) method, the power spectra density (PSD) of the velocity is obtained, as shown in Fig. 5. It is noted that the PSD in CP(T_f) is closest to that in VP. The basic frequency is 0.4 for CP(T_0), while harmonics occur for CP(T_f), CP(T_h), and VP, and the basic frequency is around 0.22. Thus, even for a very small temperature ratio, CP(T_0) still might give fairly significant errors.

Fig. 6 shows the spanwise time-mean local Nu over the heat source at different streamwise locations. The values from different models agree very well with each other. The largest discrepancy always appears at the crests in the figure, while the smallest is at the troughs. These differences are due to the combined effect of the variation in the transport properties. It is known that the crests correspond to the region where the cold fluid descends, and the trough the location where the hot fluid ascends. The fluid with a lower temperature has larger density, lower viscosity, and lower thermal conductivity. The larger density implies tendency to descend, and the lower viscosity implies greater acceleration, while the lower thermal conductivity yields lower heat flux. In this case, with $\epsilon = 0.033$, the viscosity changes more strongly than the density and the conductivity, and plays a more important role. CP(T_0) has the smallest viscosity and density, so the cold fluid around the top plate descends more easily to the heat source, and overcomes the negative effect from the thermal conductivity. This is why CP(T_0) has the largest Nu at the crests, and CP(T_h) has the smallest. However, at the troughs, where the fluid is going up, the larger density implies larger inertia, but the smaller viscosity results in greater acceleration. The opposite effects are combined, resulting in a negligible difference among all the models at the troughs. This analysis is only true for very low Re, for which the secondary convection prevails over the axial forced convection.

6. Moderate temperature ratio

The case with $\epsilon = 0.167$ is now considered. The thermal diffusivity α and the kinematic viscosity ν of air increase by about 32%, when its temperature varies from 300 to 350 K, so a pronounced discrepancy between the CP model and the VP model might be expected.

The difference in the velocity field between the CP and the VP models is presented in Fig. 7. E_{ux}, the local error in the velocity field, is defined as

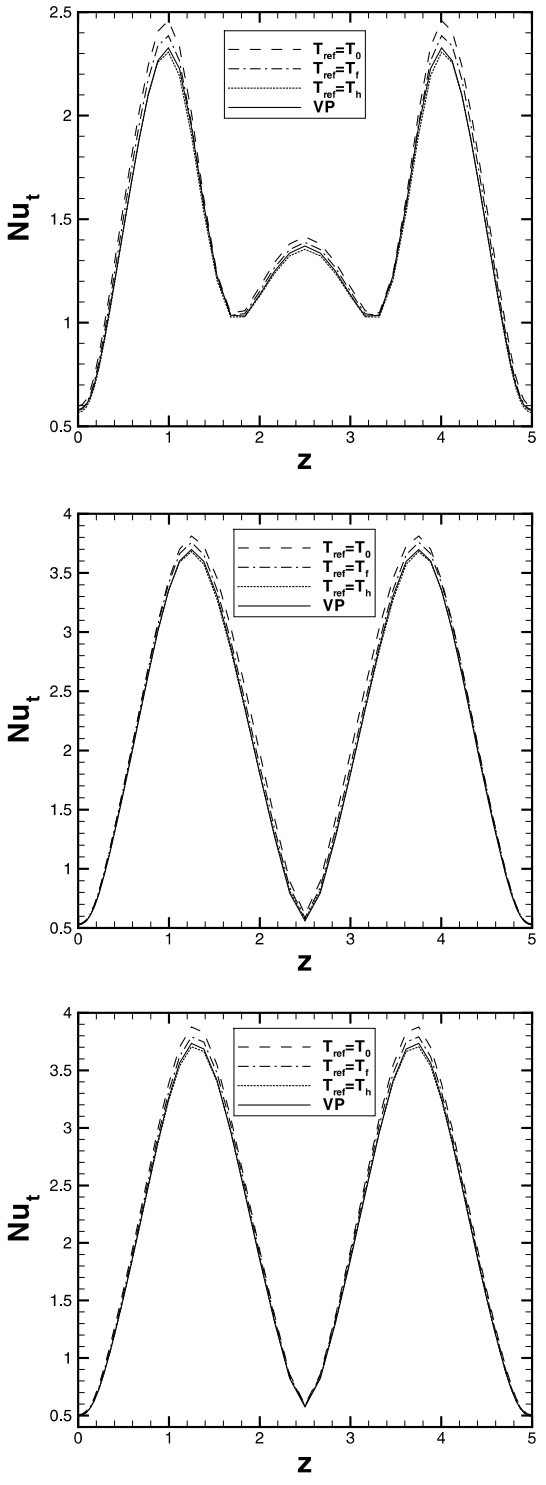

Fig. 6. Spanwise time-averaged local Nusselt number Nu_t over the heat source at three different streamwise locations, $x = 5.0$ (top figure), $x = 10.0$ (middle figure), and $x = 18.0$ (bottom figure).

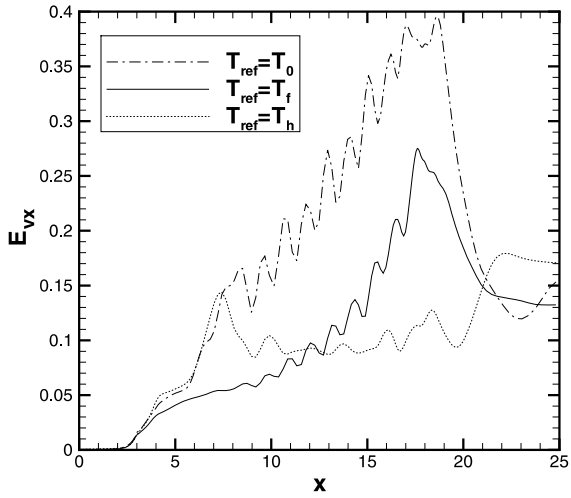

Fig. 7. Spanwise difference in the velocity between the CP models and the VP model for $Re = 50$ and $\epsilon = 0.167$.

$$E_{vx} = \frac{\oint_{cs} \sqrt{(u-u_v)^2 + (v-v_v)^2 + (w-w_v)^2}\,\mathrm{d}s}{\oint_{cs} \sqrt{u_v^2 + v_v^2 + w_v^2}\,\mathrm{d}s} \tag{27}$$

where cs represents any cross-sectional surface. In this figure, it is noted that the discrepancy in the velocity varies along the streamwise direction, and the largest error is as large as 40% for the CP(T_0) model and 28% for the CP(T_f) model. For the CP(T_0) and the CP(T_f) models, the error increases until the trailing edge of the heat source is reached and then drops very quickly. For the CP(T_h) model, the error increases over the front part of the heat source, and then keeps around 10% throughout the heat source, and finally jumps to over 15% at the trailing end of the heat source. Two main factors are involved in inducing this phenomena. One is the buoyancy, which drives the vertical motion of the fluid and distorts the velocity field from that of forced convection flow. It is expected the the velocity fields given by the CP model and the VP model, with the same initial and boundary conditions, must be exactly the same if just forced convection is involved. The other factor is the transport properties. The CP(T_0) model has the smallest viscosity everywhere, and the fluid meets smaller shear friction, resulting in a greater acceleration. With the fluid moving downstream, the average temperature of the fluid increases, which results in a larger discrepancy in the transport properties, so the error between CP(T_0) and VP increases over the heat source. Beyond the heat source, the fluid temperature drops very quickly, and the difference between the properties decreases, and the buoyancy also decreases, so the error goes down. The CP(T_f) model employs the properties at the average temperatures, and has much smaller error than CP(T_0). The CP models are not acceptable quantitatively, but may be adequate to predict qualitative

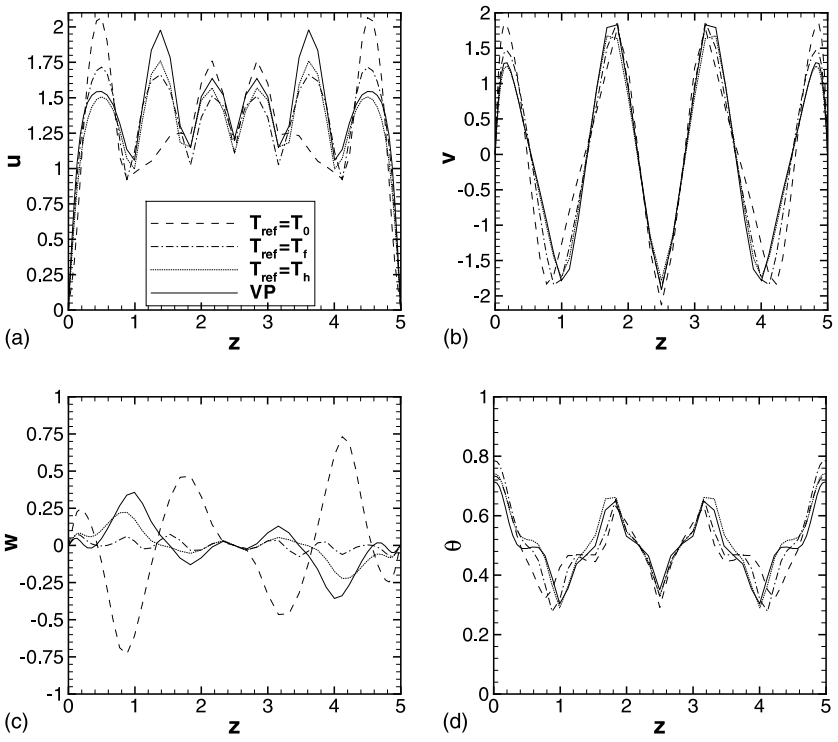

Fig. 8. Spanwise distribution of the velocity components and the temperature at $x = 15.0$ and $y = 0.5$ for $Re = 50$ and $\epsilon = 0.1667$, obtained from the different models.

trends. With integration of E_{vx} over the streamwise direction, the global average error of the velocity E_v can be obtained.

Fig. 8 shows the spanwise distribution of the velocity components and the temperature along the horizontal axis of the cross-section surface at $x = 15.0$. The distributions of v and temperature do not show a large discrepancy among the different models. The duct with a moderate height confines the vertical motion of the fluid, resulting in a smaller difference in v. The temperature distribution is determined by the vertical convection of the flow, besides the horizontal convection, so the duct height also prevents a larger difference in temperature distribution. However, the transverse velocity w has a much weaker confinement due to the side walls. As shown in Fig. 8(c), the velocity from CP(T_0) is quantitatively different from that obtained from VP, and other two CP models also deviate strongly from VP.

Fig. 9 shows the streamwise distribution of the spanwise-averaged Nusselt number. On the front part of the heat source, the Nusselt number shows the characteristics of forced convection. Then, after $x = 6.0$, the longitudinal rolls develop and improve the heat transfer, overcoming the negative effects of the upstream wake. The CP(T_f) model yields results which are quite similar to those from the VP model.

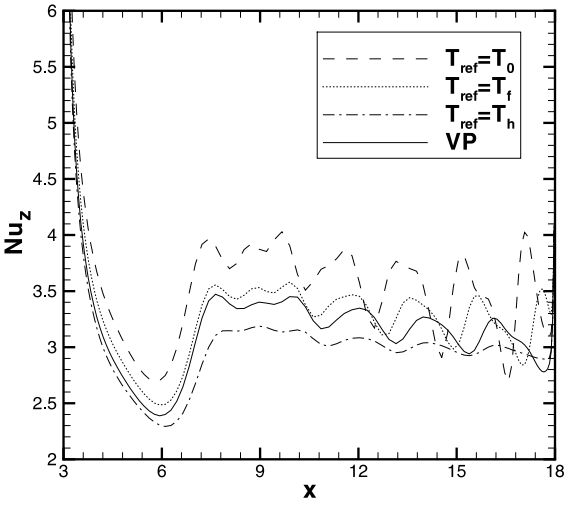

Fig. 9. Spanwise-averaged Nusselt number Nu_z from the CP models and from the VP model for $Re = 50$ and $\epsilon = 0.167$.

7. Large temperature ratio

Even for $\epsilon = 0.1667$, the CP models strongly deviate from the VP model, so a much larger discrepancy, among velocity and temperature distributions, is expected for the cases with larger temperature ratios. However, as

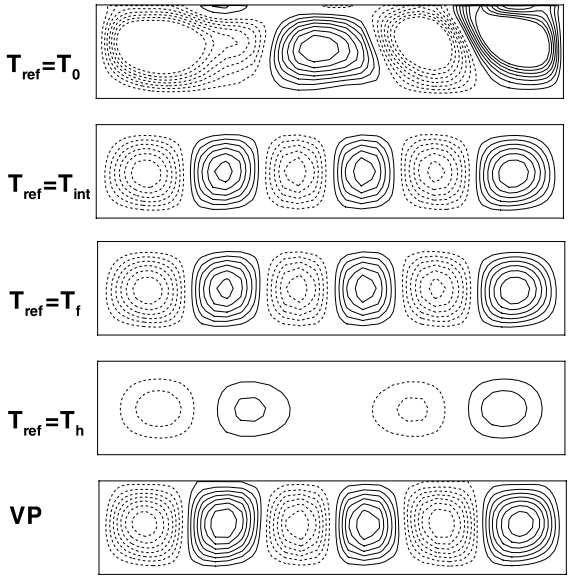

Fig. 10. Calculated sectional streamlines at $X = 18.0$ from the different models for $Re = 200$ and $\epsilon = 2.33$.

seen earlier, the CP(T_f) model can yield fairly accurate results on the Nusselt number.

Fig. 10 shows the streamlines on a cross-sectional plane at $x = 18.0$. In order to make it easy to compare the results, the contours are plotted at the same levels. Obviously, CP(T_0) does not yield a steady solution at all. The flow is in chaos, and the symmetry about the center plane is lost. All other models give steady state solutions, but CP(T_h) shows flow patterns which are very different from those yielded by other models. It is noted that the solutions given by CP(T_f) and CP(T_{int}) agree very well. The better performance of CP(T_{int}) over CP(T_f), as seen in [14], is not found here. It is surprising to find that CP(T_f) gives a reasonable solution for the Nusselt number, especially over the downstream part of the duct, as shown in Fig. 11. This results from the confinement of the flow due to the duct height, as explained earlier.

One can anticipate that good agreement between the two models might also be found for v and θ. As shown in Fig. 12, the vertical velocity component v at $x = 5.0$ has two deep grooves, which means that one pair of longitudinal rolls is generated along the side walls. Further downstream, there are a total of six rolls. The two models give very similar solutions. The temperatures calculated by CP(T_f) are higher than those by VP, both at the upstream and downstream locations in the duct. At the upstream location, $x = 5.0$, forced convection dominates, and the heat transfer in the vertical direction depends largely on thermal diffusion. The viscosity μ and the thermal conductivity k for the CP(T_f) model are larger than those for the VP model, since the average

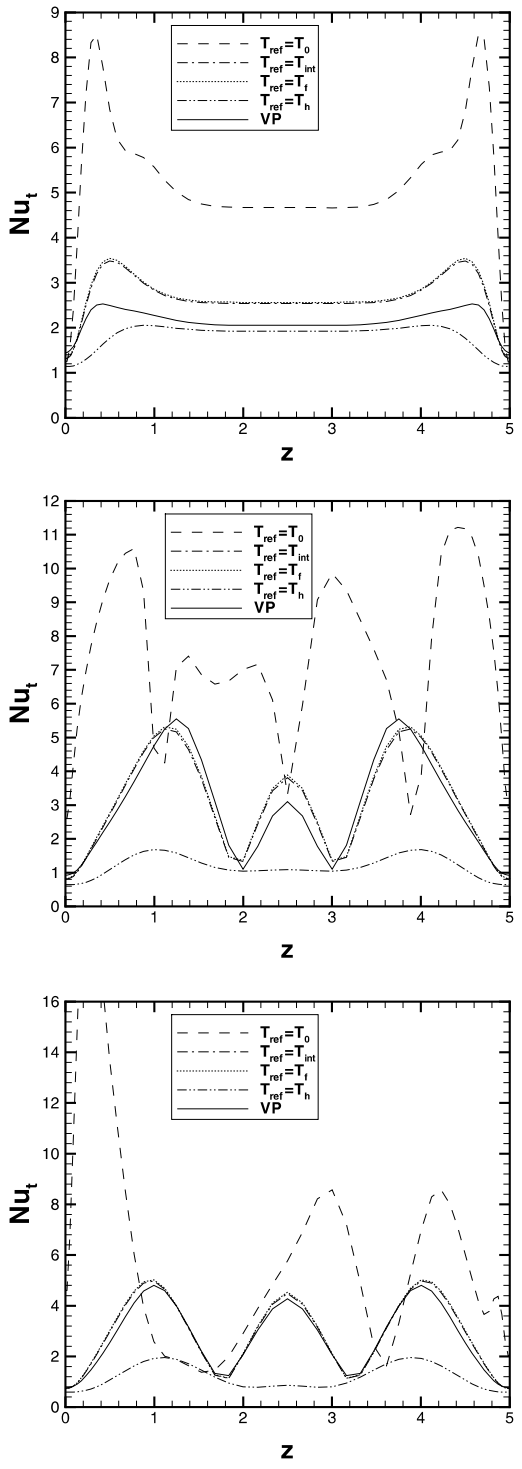

Fig. 11. Spanwise time-averaged local Nusselt number Nu_t over the heat source at three different streamwise locations, $x = 5.0$ (top figure), $x = 10.0$ (middle figure), and $x = 18.0$ (bottom figure) for $Re = 200$ and $\epsilon = 2.33$.

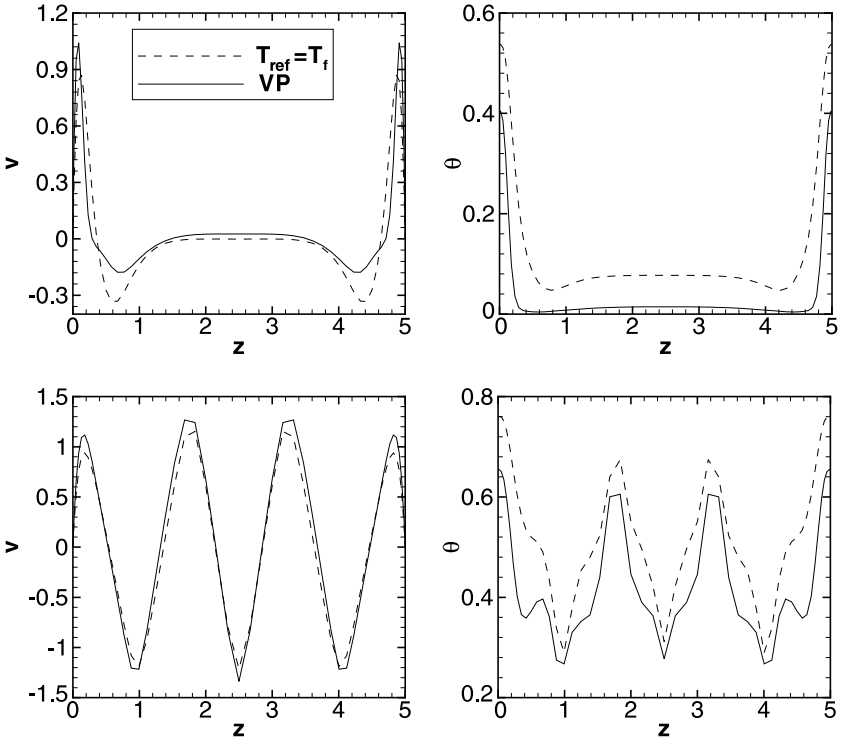

Fig. 12. Vertical velocity component v and temperature θ at $X = 5.0$, $Y = 0.5$ (top figures) and $X = 18.0$, $Y = 0.5$ (bottom figures) for $Re = 200$ and $\epsilon = 2.33$.

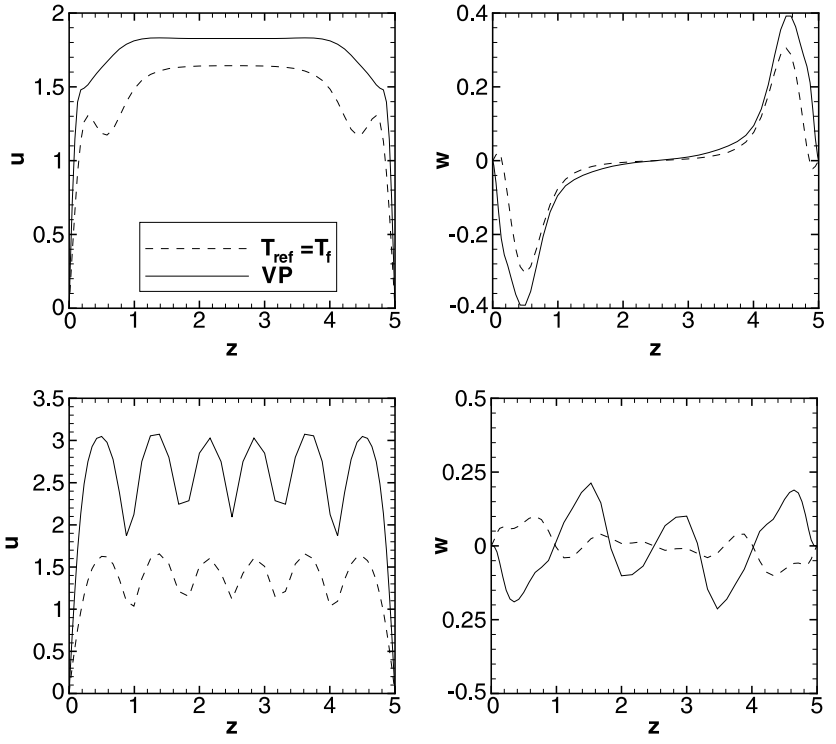

Fig. 13. Axial velocity u and transverse velocity w at $X = 5.0$, $Y = 0.5$ (top figures) and $X = 18.0$, $Y = 0.5$ (bottom figures) for $Re = 200$ and $\epsilon = 2.33$.

temperature at the upstream location is very low, far less than the average temperature T_f. The higher thermal conductivity leads to higher heat transfer, while the higher viscosity results in much lower axial velocity u, as shown in Fig. 13. The lower axial velocity gives longer time for the fluid to be heated. Thus, the CP(T_f) model predicts higher temperatures than the VP model. The inappropriateness of transport properties used by CP(T_f) also results in unacceptable error in the transverse velocity w. At $x = 5.0$, the profiles of w from both the models are similar, while they deviate from each other at the downstream location, even with opposite signs in some regions.

8. Comparison among different cases

So far, the cases with different temperature ratios have been discussed. The performance of CP models, with three different reference temperatures, are summarized in Fig. 14. CP(T_0) always gives the worst simulation among the three CP models. For the cases with $\epsilon = 0.03$ and 0.167, the CP(T_h) model has almost as good a global performance as CP(T_f), while CP(T_f) shows advantages in other cases. Even for $\epsilon = 2.33$, the global error in the Nusselt number in CP(T_f) is as low as 15%. Thus, if only the Nusselt number is of interest, CP(T_f) may be an acceptable substitute for the VP model, which requires much greater computation time. However, CP(T_f) gives a much worse simulation for the velocity field.

In order to evaluate the effects of flow conditions on the performance of the different models, the cases are studied for different Reynolds numbers, with a given temperature ratio $\epsilon = 1.0$, using CP(T_f) and VP models. The global errors in the Nusselt number and the velocity distribution are presented in Fig. 15. E_v drops almost linearly with an increase in Re. There are two reasons for this. First, a higher Re means a shorter time for the fluid through the duct, reducing the influence of the transport properties. The second reason is that, with the higher Re, forced convection effects prevail, and the secondary convection becomes weaker. Thus, the error due to the transverse velocity w reduces. The profile of E_{Nu} is different. It drops very quickly to 12%, and then stays around this value.

Fig. 16 shows the performance of CP(T_f) at $Re = 200$ for different temperature ratios. It is noted that the bigger temperature ratio leads to a higher error, because a larger temperature ratio results in a larger deviation in the fluid properties. The CP model assumes the properties are uniform, and that is not true for the cases with large temperature ratios due to the temperature dependence of the properties. It is also found that E_v is always larger than E_{Nu}, and E_v increases more quickly than E_{Nu} for $\epsilon \geqslant 0.667$.

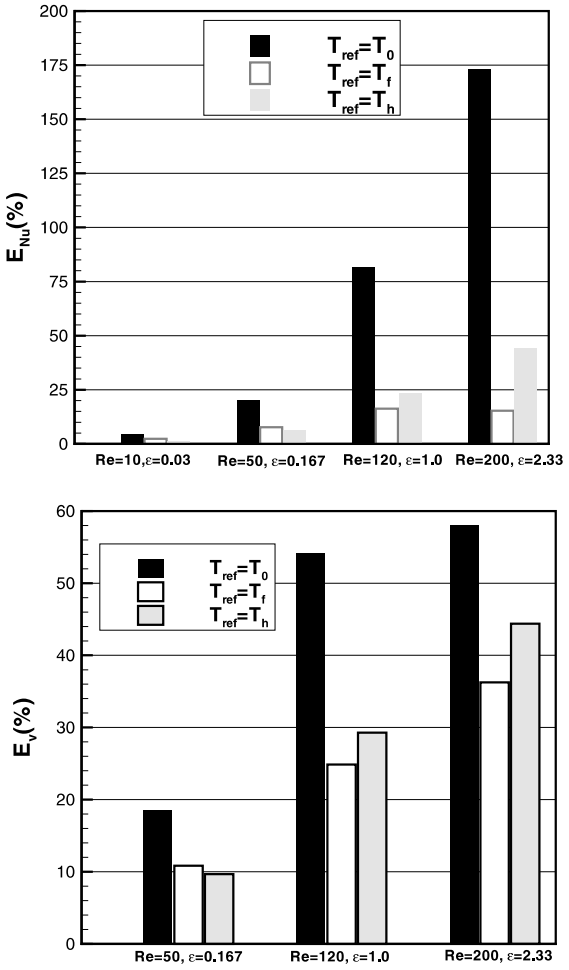

Fig. 14. Error between the CP model and the VP model in terms of the space and time-averaged Nu (top figure) and velocity (bottom figure).

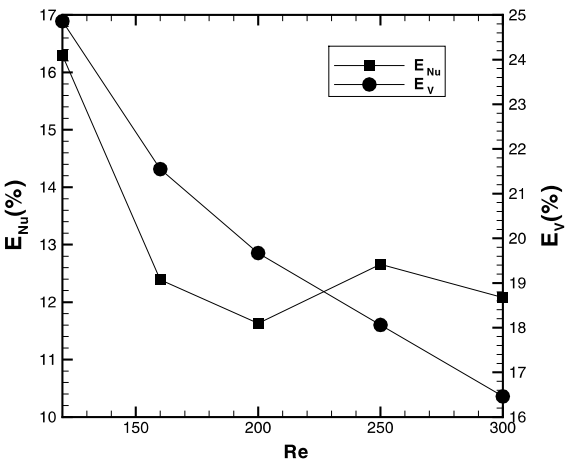

Fig. 15. The difference in Nu and velocity between CP(T_f) and VP for different Reynolds numbers at $\epsilon = 1.0$.

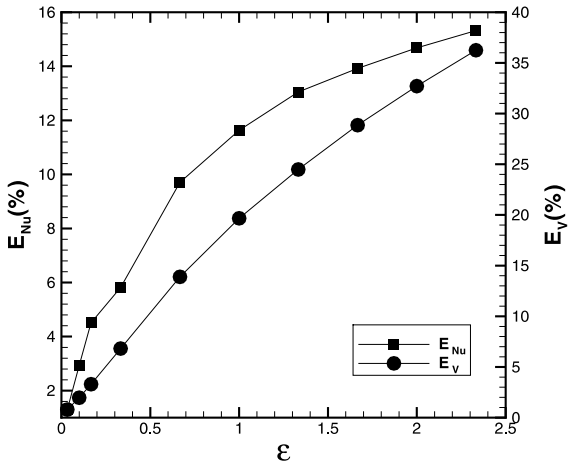

Fig. 16. The difference in Nu and velocity between CP(T_f) and VP for different temperature ratios at $Re = 200$.

9. Conclusions

The three-dimensional mixed convection flow and heat transfer in a horizontal duct under CP and VP formulations have been investigated. Among the CP models, the one based on the arithmetic average temperature T_f shows the best performance. Even for very low temperature ratios, the CP(T_0) model may yield a large error in unsteady simulations. CP(T_h) shows better performance than CP(T_0), and CP(T_{int}) has essentially the same performance as CP(T_f). The VP model is much more time-consuming than any CP model, so CP(T_f) is a reasonable choice for modest temperature ratios and even for some large temperature ratios if only the average heat transfer from the heat source is of interest.

The deviation of the predicted Nusselt numbers between CP(T_f) and VP is not so pronounced as that of the velocity fields. Both deviations decrease with an increase in Re, for a given temperature ratio, and increase with an increase in ϵ at a fixed Re.

It is also found that the discrepancies between CP(T_f) and VP in the vertical velocity component v and in the temperature θ are much smaller than those in the axial velocity u and in the transverse velocity w. Overall, it is concluded that the CP model with the average temperature as the reference is acceptable for results on steady-state heat transfer rate. However, the VP model is needed for large temperature ratios and for accurate prediction of the velocity field, particularly for unsteady flows.

Acknowledgements

Partial support from the National Science Foundation under Grant CTS-0121058 is gratefully acknowledged. Also, the support from the center for computational design (CCD) at Rutgers University is appreciated.

References

[1] S. Chandrasekhar, Hydrodynamic and Hydromagnetic Stability, Dover Publications Inc, New York, 1961, pp. 16–18.
[2] W.L. Lin, Y.T. Ker, T.F. Lin, Experimental observation and conjugated heat transfer analysis of vortex flow development in mixed convection of air in a horizontal rectangular duct, Int. J. Heat Mass Transfer 39 (1996) 3667–3683.
[3] J.T. Lir, M.Y. Chang, T.F. Lin, Vortex flow patterns near critical state for onset of convection in air flow through a bottom heated horizontal flat duct, Int. J. Heat Mass Transfer 44 (2001) 705–719.
[4] C.H. Yu, M.Y. Chang, C.C. Huang, T.F. Lin, Unsteady vortex rolls structures in a mixed convection air flow through a horizontal plane channel: a numerical study, Int. J. Heat Mass Transfer 40 (1997) 505–518.
[5] M.Y. Chang, C.H. Yu, T.F. Lin, Flow visualization and numerical simulation of transverse and mixed vortex roll formation in mixed convection of air in a horizontal flat duct, Int. J. Heat Mass Transfer 40 (1997) 1907–1922.
[6] Q. Wang, Y. Jaluria, Instability and heat transfer in mixed convection flow in a horizontal duct with discrete heat sources, Numer. Heat Transfer, in press.
[7] S. Chen, A. Lavine, Laminar buoyancy induced flow structure in a bottom heated, aspect ratio 2 duct with through-flow, Int. J. Heat Mass Transfer 39 (1996) 1–11.
[8] X. Nicolas, J.M. Luijks, J.K. Platten, Linear stability of mixed convection flows in horizontal rectangular channels of finite transversal extension heated from below, Int. J. Heat Mass Transfer 43 (2000) 589–610.
[9] K.F. Jensen, E.O. Einset, D.I. Fotiadis, Flow phenomena in chemical vapor deposition of thin films, Annu. Rev. Fluid Mech. 23 (1991) 197–232.
[10] R.E. Spall, Unsteady mixed convection in horizontal ducts with applications to chemical vapor processes, Int. Comm. Heat Mass Transfer 23 (1996) 115–122.
[11] H. Nesreddine, N. Galanis, C.T. Nguyen, Variable-property effects in laminar aiding and opposing mixed convection of air in vertical tubes, Numer. Heat Transfer Part A 31 (1997) 53–69.
[12] G. Evans, R. Greif, Unsteady three-dimensional mixed convection in a heated horizontal channel with applications to chemical vapor deposition, Int. J. Heat Mass Transfer 34 (1991) 2039–2051.
[13] G. Evans, R. Greif, Thermally unstable convection with applications to chemical vapor deposition channel reactors, Int. J. Heat Mass Transfer 36 (1993) 2769–2781.
[14] W.K.C. Chiu, Y. Jaluria, N.G. Glumac, Numerical simulation of chemical vapor deposition processes under variable and constant property approximations, Numer. Heat Transfer Part A 37 (2000) 113–132.

[15] R.K. Shah, A.L. London, Laminar Flow Forced Convection in Ducts, Academic Press Inc, New York, 1978, p. 198.
[16] D.I. Fotiadis, M. Boekholt, K.F. Jensen, Flow and heat transfer in CVD reactors: comparison of Raman temperature measurements and finite element model predictions, J. Crystal Growth 100 (1990) 577–599.
[17] K.C. Chiu, F. Rosenberger, Mixed convection between horizontal plates-I. entrance effects, Int. J. Heat Mass Transfer 30 (1987) 1645–1654.
[18] T.A. Nyce, J. Ouazzani, A.D. Daubin, F. Rosenberger, Mixed convection in a horizontal rectangular channel—experimental and numerical velocity distributions, Int. J. Heat Mass Transfer 35 (1992) 1481–1494.